Negatively charged residues adjacent to IFM motif in the DIII–DIV linker of hNa$_V$1.4 differentially affect slow inactivation

Isabelle J. McCollum[1], Yuriy Y. Vilin[1], Elizabeth Spackman, Esther Fujimoto, Peter C. Ruben*

Department of Biology, Utah State University, Logan, UT 84322, USA

Received 1 July 2003; revised 8 August 2003; accepted 8 August 2003

First published online 22 August 2003

Edited by Maurice Montal

Abstract The effects on slow inactivation (SI) of charge substitutions, neutralizations, and reversals were studied for the negatively charged residues D1309 and EE1314,15 surrounding the IFM motif in the DIII–DIV cytoplasmic linker – the putative fast inactivation particle – of human skeletal muscle voltage-gated sodium channel (hNa$_V$1.4). Changing aspartate (D) at position 1309 to glutamate (E) (substitution) did not strongly affect SI, whereas charge neutralization to glutamine (Q) and charge reversal to arginine (R) right-shifted the midpoint of the steady-state SI curve. Charge neutralization (D→Q) at position 1309 also reduced the apparent valence associated with SI. Glutamates (E) at positions 1314 and 1315 were similarly mutated. Charge reversal (EE→RR) right-shifted the steady-state SI curve and both reversal and substitution (EE→DD) reduced its apparent valence. Charge neutralization (EE→QQ) and reversal decreased the maximum probability of SI. These mutations also had differential effects on the rate of SI onset and recovery. These results suggest that charged residues in the DIII–DIV linker may interact with structures that control SI.

Key words: Sodium channel; Patch clamp; *Xenopus* oocytes

1. Introduction

Voltage-gated sodium channels (Na$_V$) are the proteins responsible for the rising phase of action potentials and for their propagation in excitable membranes. The availability of sodium channels is the primary determinant of membrane excitability. Availability is controlled by the fraction of sodium channels distributed between closed, slow-inactivated, and fast-inactivated states. Whereas the molecular bases of closed and fast-inactivated states are relatively well understood [1], a well-established concept for the molecular basis of slow inactivation (SI) has been thwarted by differences in definition and difficulties in obtaining adequate data. The data that have been obtained suggest a molecularly distributed basis for SI that includes (but is not limited to) the pore regions (p-region), the S4 voltage sensors, and the domain III–IV linker [2–5].

Fast inactivation (FI) and SI are functionally distinct. Whereas FI is important for action potential termination, spike frequency, and regulation of resting excitability, SI contributes to the activity of voltage-gated sodium channels by regulating membrane excitability, firing properties, and spike frequency adaptation [6–8]. It has also been proposed that slow processes in sodium channel inactivation might be a molecular memory mechanism that preserves traces of previous activity [9]. Whereas SI is produced either by prolonged depolarizations lasting tens of seconds or by the cumulative effect of many brief depolarizations [10], FI in sodium voltage-gated channels occurs within the time frame of a single action potential. SI and FI also have different pharmacological sensitivities. Intracellular proteolytic treatment with pronase [11] trypsin [12], α-chymotrypsin [13] or *N*-bromoacetamide [14] destroys FI but leaves SI intact. In addition, removal of FI through molecular ablation (IFM→QQQ) does not result in the removal of SI [15,16].

SI involves conformational rearrangements within the p-region [5,17] and possibly long-distance interactions with other channel structures. Based on site-directed mutagenesis studies, these other structures include S4 voltage sensors [18], which confer an apparent voltage dependence to SI [19], as well as the auxiliary β_1 subunit [2], which may alter movements of the pore itself. One theory for the mechanism underlying SI that emerges from these studies is that one or more S4 voltage sensors may undergo a slow, secondary translocation subsequent to the movement associated with activation. Such a secondary movement could lead to a collapse of the permeation pathway, perhaps involving the outer mouth of the pore. This idea is consistent with descriptions of slow (C- and P-type) forms of inactivation in voltage-gated potassium channels [20–22].

Despite the distinctions between FI and SI, these states appear to be coupled to some degree. Removal of FI by mutation of IFM to QQQ (IFM1303QQQ) in the DIII–DIV linker increases the probability of SI [15], which leads to the idea that FI may structurally limit SI, perhaps through an interaction between the FI particle and structures that underlie SI, including the p-region or the S4 voltage sensors. We hypothesized that this could be caused by electrostatic interactions between charged residues in the DIII–DIV linker and charged residues in the S4s, or by allosteric interaction between the blocking particle and the p-region. To test these hypotheses, we chose sites with negatively charged EE and D residues flanking the essential IFM motif and, using charge substituting, neutralizing and reversing mutations, attempted

*Corresponding author. Fax: (1)-435-797-1575.
E-mail address: pruben@biology.usu.edu (P.C. Ruben).

[1] These authors contributed equally to the development of this paper.

0014-5793/03/$22.00 © 2003 Published by Elsevier B.V. on behalf of the Federation of European Biochemical Societies.
doi:10.1016/S0014-5793(03)00912-8

to clarify the mechanism underlying interactions between FI and SI. We found that D1309 exerts an apparent electrostatic effect on the rate of SI, whereas EE1314,15 appears to indirectly influence kinetic and steady-state properties of SI through a combination of electrostatic and allosteric effects.

An abstract of these results has been presented [23].

2. Materials and methods

2.1. Molecular biology

Mutations at D1309 and EE1314,15 in the human skeletal muscle sodium channel ($hNa_V1.4$) DIII–DIV linker were prepared by site-directed mutagenesis using a PCR overlap extension method [24], as previously described [25]. Fig. 1 depicts the location of mutations relative to the IFM motif.

2.2. Oocyte preparation and RNA injections

Stage V–VI oocytes were surgically removed from female *Xenopus laevis* (Nasco, Modesto, CA, USA), enzymatically isolated and maintained in culture for up to 14 days at 19°C as described [2]. Approximately 24 h after enzymatic treatment, oocytes were individually injected with 27.6 nl or 50.6 nl of mRNA using an automatic injector (Nanoject, Drummond, PA, USA). Expression did not significantly differ between oocytes injected with the different amounts of mRNA. Both α- (1 μg/μl) and β_1- (3 μg/μl) subunits were injected at a volume ratio of 1:1. Before macropatch recording, the vitelline membrane was manually removed from oocytes after a short (2–3 min) exposure to a hyperosmotic solution containing (in mM): 96 NaCl, 2 KCl, 20 $MgCl_2$, 5 HEPES, 400 mannitol, pH 7.4.

2.3. Electrophysiology

All macropatch recording was done in a chamber containing (in mM): 9.6 NaCl, 88 KCl, 11 EGTA, 5 HEPES, pH 7.4. This solution was intended to zero the oocyte membrane potential. Aluminosilicate patch electrodes were fabricated (P-87, Sutter Instruments, CA, USA), dipped in melted dental wax to reduce capacitance, thermally polished, and filled with (in mM): 96 NaCl, 4 KCl, 1 $MgCl_2$, 1.8 $CaCl_2$, 5 HEPES, pH 7.4. Electrophysiological recordings were made using a patch-clamp amplifier (EPC-9, HEKA, Lambrecht, Germany), and digitized at 200 kHz via an interface (ITC-16, Instrutech, Great Neck, NY, USA). Voltage clamping and data acquisition were controlled via software (Pulse/Pulsefit, HEKA, Lambrecht, Germany) running on a G4 Power Macintosh. All data were software-low-pass-filtered at 5 kHz during acquisition. Experimental bath temperature was maintained at 22 ± 0.2°C for all experiments using a peltier device controlled by a temperature controller (HCC-100A, Dagan, Minneapolis, MN, USA). After seal formation, patches were left on-cell for all recordings. The holding potential between protocols was −100 mV. Prior to each protocol, the membrane potential was hyperpolarized to −150 mV for 30 s to recover all channels from both FI and SI. Leak subtraction was performed automatically by the software using a p/4 procedure before each protocol. Leak pulses alternated in direction from a holding potential of −120 mV.

SI was kinetically separated from FI by allowing recovery of channels from FI using a brief, hyperpolarizing pulse interposed between inactivating prepulses and test pulses. The duration and voltage required for this FI recovery pulse was determined for each mutant by analyzing the time and voltage dependence of FI recovery.

2.4. Data analysis

Analysis and graphing were done using PulseFit (Heka) and Igor Pro (Wavemetrics, Lake Oswego, OR, USA), both run on a G4 Power Macintosh. Time constants (τ) for onset and recovery of FI and SI were derived from single exponential fitting to peak current amplitude versus prepulse (or interpulse) duration using the equation:

$$I = I_{SS} + a_1 \exp(-t/\tau) \quad (1)$$

where I is current amplitude, I_{SS} is the steady-state current or asymptote (plateau amplitude), a_1 is the amplitude at time $t = 0$ (time of peak current), and τ is the time constant [2].

Where I, I_{SS} are the same as in Eq. 1 and a_1, a_2 are the amplitudes for the τ_1 and τ_2 time constants.

Steady-state SI data were fitted with a modified Boltzmann function:

$$I/I_{max} = (I_1 - I_2)/[1 + \exp(-ze_0\,(V_m - V_{1/2})/kT)] + I_2 \quad (2)$$

where I_{max} is the maximum peak current measured, I_1 and I_2 are the maximum and minimum values in the fit, V_m is the prepulse potential, $V_{1/2}$ is the midpoint voltage of the steady-state SI curve, e_0 is an elementary charge, z is apparent valence (slope factor), k is the Boltzmann constant, and T is absolute temperature. The maximum probability of SI was measured as I/I_{max} at the most depolarized voltage of the steady-state curve. For brevity, we refer to the maximum probability of steady-state SI as simply 'probability of SI'.

All statistical values, both in the text and in the figures, are given as mean ± standard error of the mean (S.E.M.). Exponential or Boltzmann fits were performed for individual data sets in order to obtain means for time constants, $V_{1/2}$ and z. Statistical differences were derived from Student's t-test or, where indicated by significant differences between standard deviations, Welch's alternate t-test, with two-tailed P values using a statistical software package (Instat, GraphPad Software, Inc., San Diego, CA, USA). Significant difference was accepted at $P < 0.05$.

3. Results

Mutations of charged residues that surround the putative FI particle in the DIII–DIV linker have been shown to alter the steady-state availability and kinetics of FI [25,26]. We have also demonstrated that there appears to be an inverse relationship between the probability of FI and the probability of SI, such that removal of FI with the IFM→QQQ mutation resulted in complete SI when, in wild-type skeletal muscle ($hNa_V1.4$) and cardiac ($hNa_V1.5$) sodium channels, the maximum probability of SI was approximately 80% and 40%, respectively [15,16]. Could this interplay between FI and SI be due to interactions between charged residues in the III–IV linker and other residues that, at least in part, control the probability of SI? We addressed this question by testing the effects of mutations of the charged residues surrounding the IFM motif on the kinetic and equilibrium parameters of SI in $hNa_V1.4$.

3.1. Kinetics of SI

We characterized the effects of mutations on voltage-dependent kinetics of development (onset) and recovery of SI. Onset of SI was studied with the pulse protocol shown by the right-hand diagram at the bottom of Fig. 1. Briefly, (1) sodium channels were hyperpolarized to −150 mV for 30 s to eliminate both FI and SI; (2) prepulses of 0–60 s (variable increments) at −70, −50, −30 and 0 mV were applied to induce SI; (3) a 20 ms pulse to −150 mV was used to selectively recover fast-inactivated channels before the test pulse; (4) the amplitudes of sodium currents elicited in response to a 0 mV test pulse were plotted as normalized current amplitude versus prepulse duration, for each interpulse voltage, and used to measure the onset of SI; (5) an additional 30 s pulse at −150 mV was used to avoid any possible accumulation of SI. Recovery from SI was studied with the pulse protocol as shown by the left-hand protocol in Figs. 1 and 2. Briefly, (1) channels were slow-inactivated by applying a 60 s prepulse to 0 mV; (2) interpulse durations of 0–60 s (variable increments) at −90, −110, and −130 mV were used to recover channels from SI; (3) a 20 ms pulse to −150 mV was used to selectively recover fast-inactivated channels before the test pulse; (4) the peak current amplitudes that were elicited by a 0 mV test pulse were plotted as normalized current amplitude

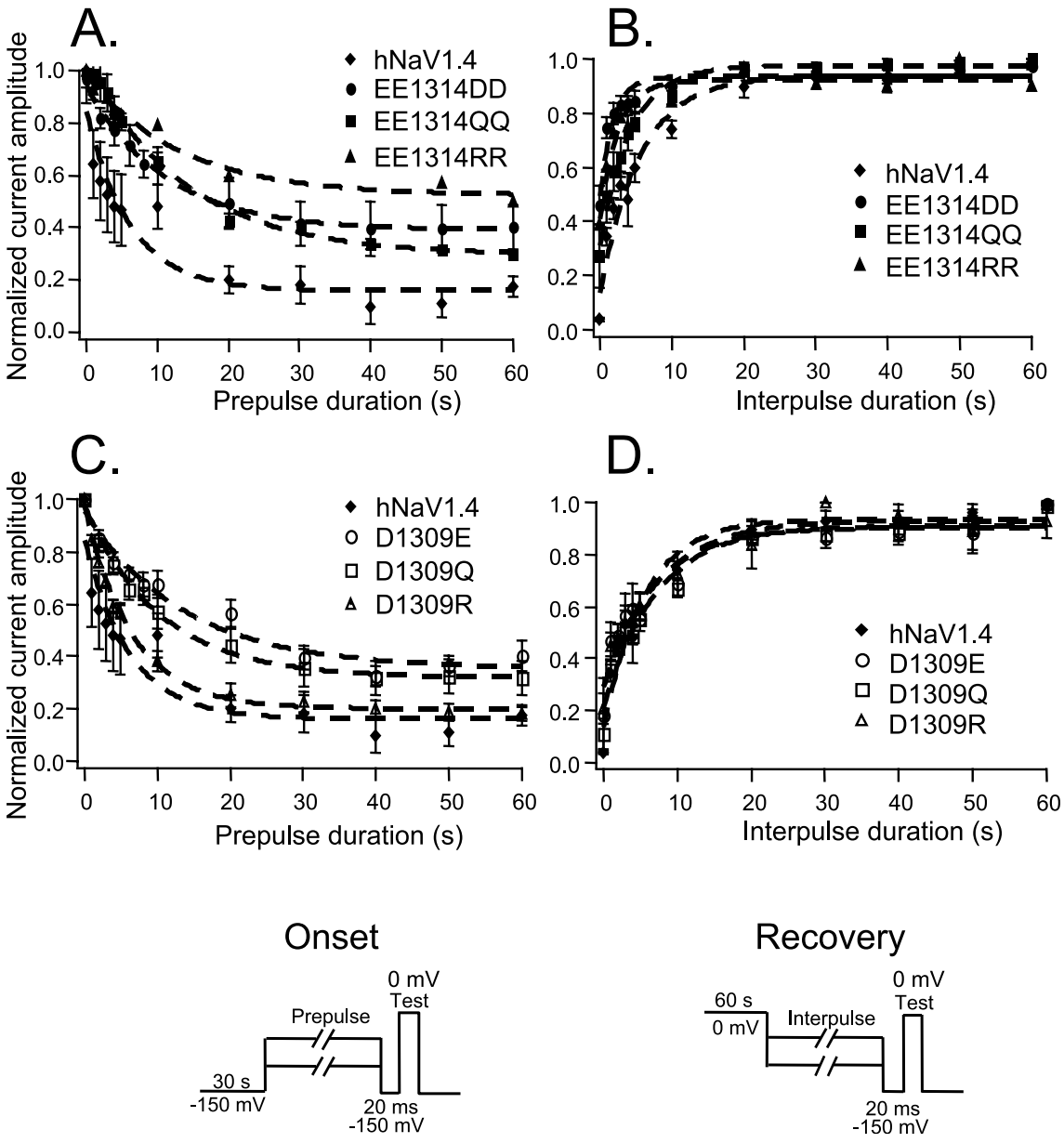

Fig. 1. Onset and recovery of SI are two-state transitions. Normalized peak current amplitudes during a 0 mV test pulse are graphed as a function of prepulse durations (panels A and C for onset – see text and left-hand pulse protocol) or interpulse durations (panels B and D for recovery – see text and right-hand pulse protocol) are shown for $hNa_V1.4$ (solid diamonds in each panel) and the mutants of residues EE1314,15 (solid symbols in panels A and B) and D1309 (open symbols in panels C and D). Single exponential functions (curves in each panel) were fit to the decay (onset) and growth (recovery) of peak current amplitude (see Eq. 1).

versus duration for each recovery voltage. Time constants (τ) for onset (and recovery) of SI were derived from monoexponential fits (see Eq. 1) of peak current amplitudes versus prepulse (or interpulse) duration, as shown in Fig. 1. The use of multi-exponential functions did not improve the fit or give time constants that were statistically different. Fig. 1A,C shows the decay of normalized peak current amplitude during inactivating 0 mV prepulses of various durations. Fig. 1B,D shows the growth of current during recovery interpulses to −130 mV for the durations shown on the *X*-axis. Time constants from the fits in Fig. 1 were subsequently plotted as a function of the prepulse or interpulse voltage, as shown in Fig. 2. Fig. 2A–C shows the voltage dependence of SI time constants in EE1314,15DD (solid circles), EE1314,15QQ (solid squares) and EE1314,15RR (solid triangles), respectively. Fig. 2D–F shows voltage dependence of SI time constants in D1309E (open circles), D1309Q (open squares) and D1309R (open triangles), respectively. The dotted line in all panels of Fig. 2 shows the SI time constants for onset and recovery from $hNa_V1.4$.

Substitution of the glutamate (E) residues at positions 1314,15 with aspartate (D) led to a decrease of SI time constants compared to wild-type channels (Fig. 2A). The effect was most pronounced at −90, −70 and −50 mV, and was accompanied by a shift of the $\tau(V)$ curve towards more positive potentials. The recovery of SI in EE1314,15DD was accelerated at −110 and −90 mV. By contrast, neutralization of the EE cluster with QQ (E1314,15QQ) did not affect maximum SI time constants (Fig. 2B). Recovery rates were also not significantly different. The rate of onset in EE1314,15QQ,

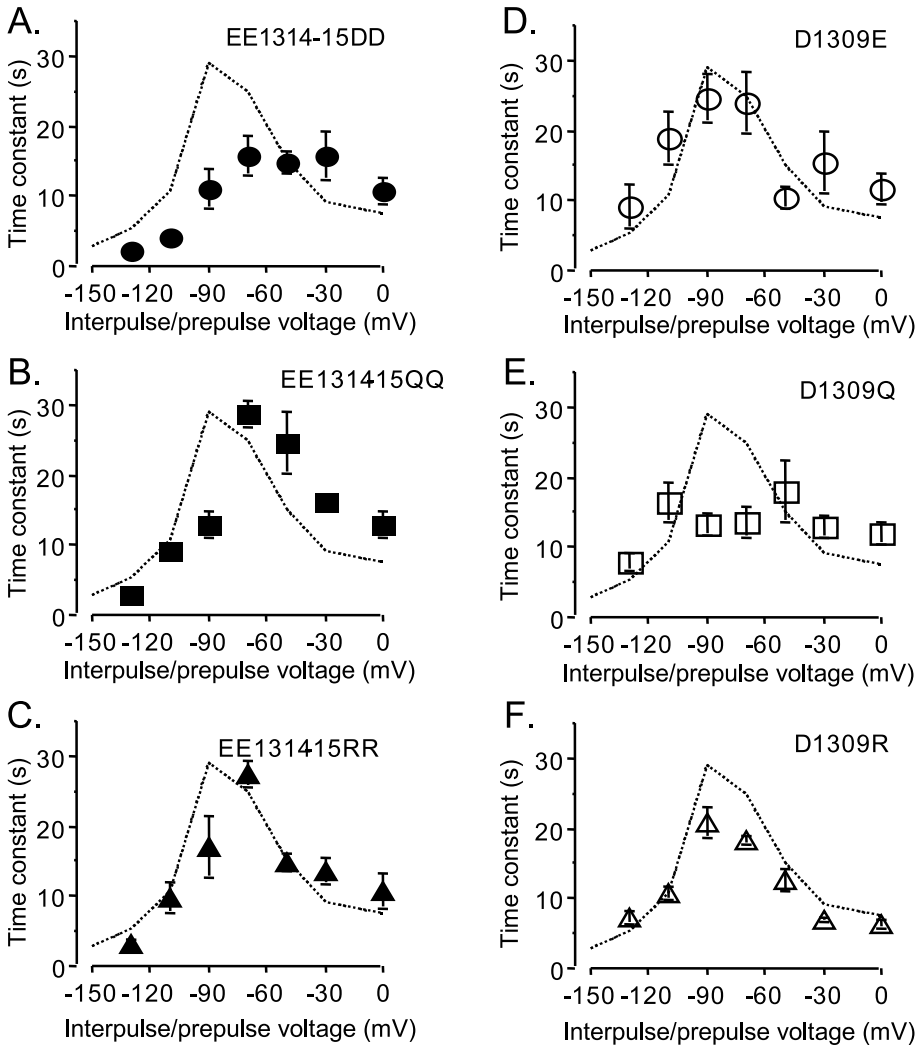

Fig. 2. Effects of DIII–DIV mutations on SI time constants. In each panel, hNa$_V$1.4 data is shown as a dashed line. A–C: The averaged time constants for SI in EE1314,15DD (solid circles), EE1314,15QQ (solid squares), and EE1314-14RR (solid triangles). D–F: The averaged time constants for SI in D1309E (open circles), D1309Q (open squares), and D1309R (open triangles). All data derived from single exponential fits to SI recovery and SI onset. Time constants are plotted versus the prepulse or interpulse voltage. Pulse protocols were as shown in Fig. 1. All values represent mean ± S.E.M.

however, differed from that of wild-type channels at −50, −30 and 0 mV. Reversal of negative charge in the 1314,15 EE cluster to positively charged arginines (EE1414,15RR, Fig. 2C) caused no significant changes in the voltage dependence of SI time constants.

Charge substitution and charge reversal at the D1309 site (D1309E, Fig. 2D, and D1309R, Fig. 2F, respectively) had no significant effect on SI time constants. However, neutralization of negative charge (D1309Q, Fig. 2E) significantly decreased onset time constants at −90 and −70 mV. The rates of recovery from SI were not altered by D1309Q.

3.2. Steady-state probability of SI

When channels enter the slow-inactivated state they become unavailable for activation. In other words, the total number of channels available to generate and propagate action potentials decreases, which leads to a decrease of membrane excitability. The relative number of channels that has been 'slowly' inactivated can be evaluated by assessing the steady-state distribution of SI. The diagram at the bottom of Fig. 3 shows the pulse protocol used to measure steady-state SI. Briefly, prepulses were alternated to avoid time-related artifacts; first, the voltage was stepped to all 'even' voltages (e.g. −160, 0, −140, −20 mV etc.); next the voltage was stepped to all 'odd' voltages (e.g. −150, +10, −130, −10 mV etc.) to encompass the full range of prepulse potentials from −160 mV to +10 mV. Before every SI prepulse, 30 s at −150 mV was allowed to insure complete recovery from all previous inactivation to avoid accumulation of inactivation. The prepulse duration for steady-state SI was 1 min. A 20 ms pulse at −150 mV was interposed between the prepulse and the test pulse (0 mV) to allow full recovery of fast-inactivated channels. Data were normalized to the peak current amplitude and plotted as a function of prepulse voltage. All values for maximum probability (%), midpoint ($V_{1/2}$) and apparent valence (z) are shown in Table 1.

Fig. 3A shows the averaged steady-state distribution of SI in hNa$_V$1.4 (solid diamonds, $n = 10$) plotted as current amplitude versus 60 s prepulse voltage and normalized to the current recorded from the most hyperpolarized prepulse voltage.

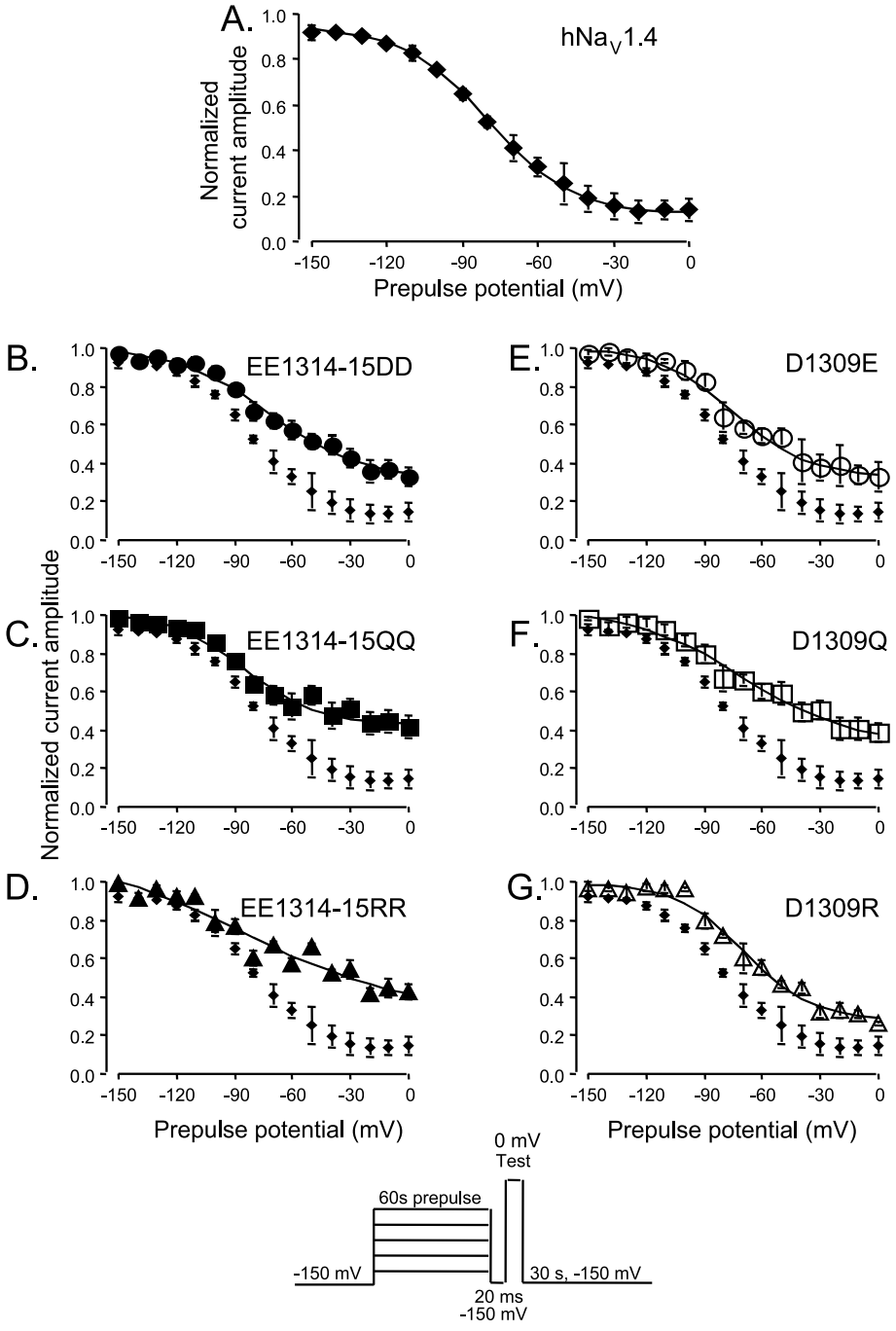

Fig. 3. Charge neutralization and charge reversal in EE cluster alters steady-state probability of SI. A: The steady-state SI in hNa$_V$1.4 (solid diamonds). B–D: The steady-state SI in EE1314,15DD (solid circles), EE1314,15QQ (solid squares) and EE1314,15RR (solid triangles), respectively. E–G: The steady-state SI for D1309E (open circles), D1309Q (open squares) and D1309R (open triangles), respectively. In all graphs steady-state inactivation is plotted as average normalized current amplitude versus 60 s prepulse voltage. Solid diamonds represent averaged steady-state SI in hNa$_V$1.4 in all panels of this figure. The inset represents steady-state protocols for these data. Numerical values for midpoint, apparent valence and maximum probability are summarized in Table 1.

All panels in Fig. 3 include the average steady-state SI data from hNa$_V$1.4 channels for comparison, shown as the diamonds in Fig. 3B–G. Fig. 3B demonstrates that the EE1314,15DD mutation does not significantly affect the probability of SI relative to wild-type hNa$_V$1.4 channels ($P > 0.2$). However, the steady-state curve in EE1314,15DD has a significantly lower slope than hNa$_V$1.4 channels ($P < 0.001$). In addition, the EE1314,15DD steady-state inactivation midpoint was significantly shifted to more depolarized potentials relative to hNa$_V$1.4 ($P < 0.05$). Neutralizing the negative charges in EE1314,15QQ (solid squares, Fig. 3C) decreases the probability of SI ($P < 0.05$). The midpoint and slope are not significantly altered in EE1314,15QQ ($P > 0.5$ and 0.5, respectively). The charge reversal mutation, EE1314,15RR, (solid triangles, Fig. 3D) also has variable effects on steady-state SI. The maximum probability of SI in EE1314,15RR was significantly decreased ($P < 0.03$ Also, EE→RR significantly lowers the apparent valence of steady-state inactivation

Table 1
Inactivation parameters for $hNa_V1.4$, and mutants

Channel	SI			FI[a]	
	Probability (%)	$V_{1/2}$ (mV)	Slope factor (z)	$V_{1/2}$ (mV)	Slope factor (z)
$hNa_V1.4$ ...**KD***IFM*T**EE**Q...	80 ± 5 (10)	−83 ± 4 (10)	−1.45 ± 0.09 (10)	−94.6 ± 1.8	4.34 ± 0.11
D1309R ...**KR***IFM*TEEQ...	81 ± 2 (4)	−64 ± 2 (4)[b]	−1.31 ± 0.09 (4)	−82.0 ± 1.0[b]	4.37 ± 0.15
D1309Q ...**KQ***IFM*TEEQ...	68 ± 5 (4)	−67 ± 3 (4)[b]	−0.91 ± 0.05 (4)[b]	−93.8 ± 1.3	3.90 ± 0.13[b]
D1309E ...**KE***IFM*TEEQ...	70 ± 4 (4)	−80 ± 3 (4)	−1.42 ± 0.3 (4)	−88.7 ± 1.3[b]	5.11 ± 0.11[b]
EE1314RR ...KD*IFM*T**RR**Q...	59 ± 5 (4)[b]	−74 ± 3 (4)	−1.00 ± 0.12 (4)[b]	−101.9 ± 1.7[b]	3.98 ± 0.07[b]
EE1314QQ ...KD*IFM*T**QQ**Q...	60 ± 4 (4)[b]	−80 ± 3 (4)	−1.27 ± 0.25 (4)	−97.7 ± 0.9	4.42 ± 0.06
EE1314DD ...KD*IFM*T**DD**Q...	71 ± 5 (5)	−70 ± 2 (5)[b]	−1.01 ± 0.04 (5)[b]	−98.3 ± 1.2	4.33 ± 0.08

Values are ± S.E.M (n).
[a]Data from [25].
[b]Denotes mutant statistically different than $hNa_V1.4$.

($P < 0.02$). By contrast, the midpoint of steady-state inactivation was not significantly shifted by EE1314,15RR ($P > 0.1$).

A similar series of experiments with D1309E (charge substitution), D1309Q (charge neutralization), and D1309R (charge reversal) demonstrated no significant effect of these mutations on the probability of SI relative to $hNa_V1.4$ ($P > 0.2$, 0.1 and 0.8, respectively). The midpoint and apparent valence in D1309E are also not significantly different from those of $hNa_V1.4$ channels ($P > 0.9$ and 0.8, respectively). Although D1309R (Fig. 3G, open triangles) has no effect on the probability of SI or the slope factor ($P > 0.9$ and 0.3), the midpoint voltage of SI was significantly depolarized ($P < 0.001$). The charge neutralization D1309Q also significantly depolarized the midpoint voltage ($P < 0.03$) and decreased the apparent valence relative to $hNa_V1.4$ ($P < 0.004$). These results suggest that D1309 may interact with the structures that control the voltage dependence of SI.

4. Discussion

Does the III–IV linker interact with structures that control SI? Our earlier experiments suggest that this might be the case, since removal of FI with the IFM→QQQ mutation stabilizes the slow inactivated state in skeletal muscle and cardiac sodium channels [15,16]. This study sought to clarify the molecular mechanisms by which the DIII–DIV linker might affect SI. We focused on the charges surrounding the IFM putative inactivation particle (D1309 and EE1314,15) because mutations of the charged residues surrounding the IFM motif have been shown to affect the voltage-dependent rates of inactivation and deactivation [25]. Our results show that mutations at 1309 and1314,1315 have differential effects on properties of SI. Charge reversal (EE→RR) and charge neutralization (EE→QQ) at positions 1314 and 1315 decreased the probability of SI. Since this decrease was not observed with charge replacement (EE→DD), the effects of charge reversal and neutralization suggest that the probability of SI is dependent, at least in part, on the interactions between charges adjacent to the IFM motif and the structures that regulate the probability of SI. This result supports our earlier observation that molecular ablation of FI by the IFM→QQQ mutation increases the probability of SI due to a reciprocal interaction between FI and SI [15,16]. Groome et al. [25] demonstrated that EE→RR significantly stabilized steady-state FI and EE→QQ produced a similar but lesser effect. The destabilization of SI (shown by the present data) in the same mutants that stabilize FI (in [25]) is again consistent with our previous results in which mutagenic removal of FI stabilized SI [15,16]. Other mutations destabilized FI (right-shifted h_∞ curves in D1309R and D1309E) or had no effect on the steady-state distribution of fast-inactivated channels [25]. These minor effects on FI are consistent with the statistically insignificant effects of the mutations at position 1309 on the probability of SI in the present study.

We have previously demonstrated that the probability of SI is controlled, at least in part, by the pore structure [2,5]. By contrast, the S4 voltage sensors do not profoundly affect the probability of SI. Instead, the voltage sensors have a greater effect on the rate of entry into and recovery from the slow-inactivated state [18,27]. The strongest effects of the DIII–DIV linker mutations that were studied here were on the rate of SI. Taken together, the results from the present results are consistent with previous studies [25,28] in which mutations in the DIVS4 and the III–IV linker affect voltage-dependent gating transitions. Charged residues in the III–IV linker thus appear to influence the rate and, to a lesser extent, the steady-state probability of SI. This idea does not run counter to the conclusion that FI and SI are not mutually exclusive states [29]. Rather, they reinforce, and suggest a physical basis for, the hypothesis that fast- and slow-inactivated states are reciprocally interactive: an decrease in the stability of SI is concomitant with an increase in the stability of FI.

A physical model of the interactions between FI and SI that evolves from these studies is that docking of the IFM particle during FI impedes the subsequent pore transitions that result in SI [22]. Thus, the probability of SI is increased in the absence of FI (produced by ablation of the IFM triad). Conversely, the probability of SI is decreased by the mutations studied here, which were previously shown to stabilize FI [25]. The present study suggests that the rate at which the IFM particle reaches its final, FI-favored position is controlled in part by the charges in the III–IV linker, perhaps through a combination of electrostatic and allosteric interactions with the S4 voltage sensors or the S4–S5 linkers which, in DIII and DIV, have been proposed to act as docking sites for as yet unidentified residues in the DIII–DIV linker [30,31]. These interactions, in turn, appear to limit the rate of SI. The idea that residues in the DIII–IV linker interact with the putative DIII and DIV S4–S5 docking sites has been previously suggested vis-à-vis ultra-SI [32]. FI and ultra-SI also appear to be reciprocally interactive. Double mutations, in which both the residues studied here and those in the putative docking sites or in the voltage sensors themselves, will help to further clarify the nature and location of these interactions.

Acknowledgements: The authors gratefully thank Jennifer Abbruzzese and James Groome for critically reading the manuscript, and Elena Vilin for technical assistance. We further thank Dr. James Groome for the use of his data on fast inactivation in Table 1. This project was supported by PHS grant R-01 NS29204 to P.C.R.

References

[1] Catterall, W.A. (2000) Neuron 26, 13–25.
[2] Vilin, Y.Y., Makita, N., George, A.L. and Ruben, P.C. (1999) Biophys. J. 77, 1384–1393.
[3] Mitrovic, N., George, A.L. and Horn, R. (2000) J. Gen. Physiol. 115, 707–717.
[4] Ong, B.-H., Tomaselli, G.F. and Balser, J.R. (2000) J. Gen. Physiol. 116, 653–661.
[5] Vilin, Y.Y., Fujimoto, E. and Ruben, P.C. (2001) Biophys. J. 80, 2221–2230.
[6] Ruff, R.L., Simoncini, L. and Stuhmer, W. (1988) Muscle Nerve 11, 502–510.
[7] Sawczuk, A., Powers, R.K. and Binder, M.C. (1995) J. Neurophysiol. 73, 1799–1810.
[8] Fleidervish, I.A., Freidman, A. and Gutnick, M.J. (1996) J. Physiol. 493, 83–97.
[9] Toib, A., Lyakhov, V. and Marom, S. (1998) J. Neurosci. 18, 1893–1903.
[10] Struyk, A. and Cannon, S. (2003) Biophys. J. 84, 69a.
[11] Rudy, B. (1978) J. Physiol. 283, 1–21.
[12] Starkus, J.G. and Shrager, P. (1978) Am. J. Physiol. 235, C238–C244.
[13] Valenzuela, C. and Bennett, P.B. (1994) Biophys. J. 67, 161–171.
[14] Salgado, V.L., Yeh, J.Z. and Narahashi, T. (1985) Biophys. J. 47, 567–571.
[15] Featherstone, D.E., Richmond, J.E. and Ruben, P.C. (1996) Biophys. J. 71, 3098–3109.
[16] Richmond, J.E., Featherstone, D.E., Hartmann, H.A. and Ruben, P.C. (1998) Biophys. J. 74, 2945–2952.
[17] Townsend, C. and Horn, R. (1997) J. Gen. Physiol. 110, 23–33.
[18] Kontis, K.J. and Goldin, A.L. (1997) J. Gen. Physiol. 110, 403–413.
[19] Ruben, P.C., Starkus, J.G. and Rayner, M.D. (1990) Biophys. J. 58, 1169–1181.
[20] Loots, E. and Isacoff, E.Y. (1998) J. Gen. Physiol. 112, 377–389.
[21] Loots, E. and Isacoff, E.Y. (2000) J. Gen. Physiol. 116, 623–635.
[22] Jiang, X.J., Bett, G.C.L., Li, X.Y., Bondarenko, V.E. and Rasmusson, R.L. (2003) J. Physiol. 548, 683–695.
[23] Spackman, E., Fujimoto, E., Vilin, Y.Y. and Ruben, P.C. (2002) Biophys. J. 78, 84A.
[24] Ho, H.N., Hun, H.D., Morton, R.M., Pullen, J.K. and Pease, L.R. (1989) Gene 77, 51–59.
[25] Groome, J.R., Fujimoto, E. and Ruben, P.C. (2003) J. Physiol. 548, 85–96.
[26] Moorman, J.R., Kirsch, G.E., Brown, A.M. and Joho, R.H. (1990) Science 250, 688–691.
[27] Vilin, Y.Y., McCollum, I.J., Fujimoto, E. and Ruben, P.C. (2003) Biophys. J. 84, 215a–216a.
[28] Kuhn, F. and Greef, N. (1999) J. Gen. Physiol. 114, 167–183.
[29] Vedantham, V. and Cannon, S.C. (1998) J. Gen. Physiol. 111, 83–93.
[30] Smith, M.R. and Goldin, A.L. (1997) Biophys. J. 73, 1885–1895.
[31] Mitrovic, N., Lerche, H., Heine, R., Fleischhauer, R., Pika-Hartlaub, U., Hartlaub, U., George, A.L. and Lehmann-Horn, F. (1996) Neurosci. Lett. 214, 9–12.
[32] Hilber, K. et al. (2002) J. Biol. Chem. 277, 37105–37115.